JOURNAL OF GEOPHYSICAL RESEARCH, VOL. 114, A05207, doi:10.1029/2009JA014048, 2009

Response of ions of ionospheric origin to storm time substorms: Coordinated observations over the ionosphere and in the plasma sheet

M. Nosé,[1] S. Taguchi,[2] S. P. Christon,[3] M. R. Collier,[4] T. E. Moore,[4] C. W. Carlson,[5] and J. P. McFadden[5]

Received 5 January 2009; revised 10 February 2009; accepted 4 March 2009; published 12 May 2009.

[1] We investigate variations of ion flux over the ionosphere and in the plasma sheet when storm time substorms are initiated, using simultaneous observations of neutral atoms in the energy range of up to a few keV measured by the low-energy neutral atom (LENA) imager on board the Imager for Magnetopause-to-Aurora Global Exploration (IMAGE) satellite, outflowing ion flux of <1 keV measured by the ion electrostatic analyzer (IESA) on board the Fast Auroral SnapshoT (FAST) satellite, and energetic (9–210 keV/*e*) ion flux measured by the energetic particle and ion composition (EPIC) instrument on board the Geotail satellite. We examined three storm intervals during which the IMAGE or FAST satellite was in a suitable location to observe ionospheric ion outflow and the Geotail satellite was in the plasma sheet on the nightside. The neutral atom flux observed by IMAGE/LENA in the first interval and outflowing ion flux observed by FAST/IESA in the second and third intervals indicate that storm time substorms can cause increases of low-energy ion flux over the ionosphere by a factor of 3–50 with time delay of less than several minutes. In the plasma sheet, the flux ratio of O^+/H^+ is rapidly enhanced at the storm time substorms and then increased gradually or stayed at a constant level in a time scale of ~1 h, suggesting a mass-dependent acceleration of ions at local dipolarization and a subsequent additional supply of O^+ ions to the plasma sheet which have been extracted from the ionosphere at the substorms. These coordinated observations revealed that substorms have both an immediate effect and a delayed effect (i.e., two-step effect) on the ion composition in the plasma sheet.

Citation: Nosé, M., S. Taguchi, S. P. Christon, M. R. Collier, T. E. Moore, C. W. Carlson, and J. P. McFadden (2009), Response of ions of ionospheric origin to storm time substorms: Coordinated observations over the ionosphere and in the plasma sheet, *J. Geophys. Res.*, *114*, A05207, doi:10.1029/2009JA014048.

1. Introduction

[2] Recent studies revealed the ionosphere as an important source of plasma to the plasma sheet and the magnetosphere. *Moore* [1991] proposed a boundary called "density geopause," within which the ionospheric source is the dominant contributor to the plasma. According to the multifluid MHD simulation by *Winglee* [1998], the density geopause can be extended down the tail to 10–65 R_E during the southward IMF (B_Z = 0 to −5 nT). A large number of numerical simulations were performed to trace ions of ionospheric origin after they escaped from the ionosphere [e.g., *Delcourt et al.*, 1999; *Chappell et al.*, 2000; *Cully et al.*, 2003a]. They found that most of such ions preferentially move into the plasma sheet. Thus it is important to identify by observations how much ions are outflowing from the ionosphere and how it depends on the geomagnetic disturbances.

[3] Using the Dynamic Explorer (DE) 1 observation of low-energy (0.01–17 keV) ions at altitudes of 16000–23000 km, *Yau et al.* [1985, 1988] found a good correlation between the ion outflow rate and the Kp index. As the Kp index increased from 0 to 6, the O^+ flux increased drastically by an order (from $1–3 \times 10^{25}$ s^{-1} to $1–3 \times 10^{26}$ s^{-1}), while the H^+ flux changed by a factor of ~3 (from 3×10^{25} s^{-1} to 1×10^{26} s^{-1}). With the similar data set from DE 1, *Kondo et al.* [1990] revealed that the occurrence frequency of various types of upflowing ions (beams, conics, and hybrid types) increases much more rapidly with Kp for O^+ than H^+. From observations of ion outflow in the energy range of <20 eV at 6000–9000 km altitude by the EXOS-D satellite, *Abe et al.* [1996] found that the O^+ flux integrated over 60°–75° invariant latitude increases with the Kp index by a factor of ~5 from Kp = 1 to 7. Extending the study of Abe et al., *Cully et al.* [2003b] showed that ion outflow rate is correlated

[1]Data Analysis Center for Geomagnetism and Space Magnetism, Graduate School of Science, Kyoto University, Kyoto, Japan.
[2]Department of Information and Communication Engineering, University of Electro-Communications, Chofu, Japan.
[3]Focused Analysis and Research, Columbia, Maryland, USA.
[4]NASA Goddard Space Flight Center, Greenbelt, Maryland, USA.
[5]Space Sciences Laboratory, University of California, Berkeley, California, USA.

0148-0227/09/2009JA014048$09.00

with the Kp index and some solar wind parameters. They concluded that the Kp dependence of H^+ and O^+ flux was almost similar to that by *Yau et al.* [1985, 1988]; and that the solar wind parameters exhibiting a strong correlation with the outflow flux were the kinetic pressure, the electric field, and the variation in the IMF. In these previous studies the 3-h Kp index or the hourly averaged solar wind data (OMNI data) have been used, suggesting that the reported good correlation is correct only in a statistical or average sense. From these results, it is not clear how the outflowing ion flux responds to geomagnetic disturbances in a shorter time scale (<1 h).

[4] Some recent studies investigated a short time response of the outflowing ion flux to auroral activities. Using the measurements by the ion electrostatic analyzer (IESA) on board the Fast Auroral SnapshoT (FAST) satellite, *Tung et al.* [2001] examined the outflow flux during the 2 h interval which is centered at substorm onset determined by the Polar/UVI images. A peak of the outflow flux was found to appear frequently after substorm onset (within 10–40 min after onset; see their Figure 2). *Wilson et al.* [2001] also used the FAST/TEAMS and Polar/UVI data statistically, and found that the time delay between auroral intensification and the most intense fluxes of escaping O^+ ions is 5–12 min. The similar but longer-term data set of the FAST and Polar satellites led *Wilson et al.* [2004] to conclude that the ion outflow rate at the nightside auroral zone reached its peak level about 20 min after auroral brightenings, which is about 1.5–2 times larger than the preonset level. It should be noted that the above studies focused on time delay between auroral onset and peak time of outflowing ion flux, and the time delay was supposed to be 10–20 min.

[5] In this study we intended to investigate how quickly ion outflow rate responds to individual substorms, using data obtained by the low-energy neutral atom (LENA) imager on board the Imager for Magnetopause-to-Aurora Global Exploration (IMAGE) satellite and the FAST/IESA instrument. Moreover, in order to investigate how the plasma sheet ion composition changes during the identical substorm, we examined simultaneous observations of energetic (9–210 keV/*e*) ion flux in the plasma sheet made by the energetic particle and ion composition (EPIC) instrument on board the Geotail satellite.

[6] The rest of this paper is organized as follows. Section 2 introduces the data set. In section 3 we describe the event selection procedure. We found 3 intervals during which the IMAGE (or FAST) and Geotail satellites simultaneously observed ions of ionospheric origin over the ionosphere and in the plasma sheet. In section 4 satellite observations will be displayed for the these intervals. It was found that substorms caused rapid increases of both the outflowing ion flux above the ionosphere and the O^+/H^+ energy density ratio in the plasma sheet. The O^+/H^+ ratio subsequently increased or stayed at a constant level with a time scale of 1 h. We will discuss these observational results in section 5.

2. Instrumentation and Data Set

2.1. Measurement of Outflowing Ions Over the Ionosphere

[7] The IMAGE satellite is a polar orbiting satellite with a perigee of 1000 km altitude, an apogee of 8.2 R_E, and an orbital period of 14.2 h [*Burch*, 2000]. The satellite spins at a rate of ~0.5 revolution per minute and its spin vector is antiparallel to the orbital angular momentum vector. The LENA imager carried by the IMAGE satellite is designed to detect neutral atoms in the energy range of ~10 eV to a few keV with mass information [*Moore et al.*, 2000]. In this study we utilized data combining the H and O peaks in the time-of-flight spectrum. The LENA imager has a field of view of ±45° against a satellite spin plane which is divided into 12 polar sectors. Because of the spin, the imager sweeps out 360° in azimuthal direction which is divided into 45 azimuthal sectors. This results in one 2-D complete image of neutral atom flux covering an area of 90°(polar) × 360°(azimuth) with a nominal 8° × 8° angular resolution at every 2 min. Low-energy neutral atoms traveling from the direction of the Earth are created by charge exchange processes from outflowing ionospheric ions, which are observed at altitude higher than 2000–5000 km [*Ghielmetti et al.*, 1978; *Gorney et al.*, 1981; *Moore et al.*, 1986]. Thus we can investigate temporal change of the low-energy ion flux over the ionosphere from the LENA data.

[8] The FAST satellite was launched on 21 August 1996 into an 83° inclination elliptical orbit with a perigee of 350 km altitude and an apogee of 4175 km altitude [*Carlson et al.*, 1998]. Its orbital plane evolves throughout the year, thus the satellite covers wide ranges of latitude, local time, and seasons. The FAST satellite carries the IESA instruments which measure ion flux over the energy range from 3 eV to 25 keV in 48 energy steps [*Carlson et al.*, 2001]. The IESA instruments are mounted on opposite sides of the satellite in pair and have 12°(polar) × 180°(azimuth) field of view individually, resulting in coverage of an unobstructed 360° field of view in the azimuthal direction within the spin plane. This 360° field of view is divided by 32 angular bins. Since the Earth's magnetic field lies in the spin plane within a few degrees in the auroral zone, a full pitch angle distribution of ions can be obtained with angular resolution of ~11°. Original time resolution for one complete measurement (i.e., ion flux in 48 energies and 32 pitch angles) is 78 ms, but in this study we used 5-s average data.

2.2. Measurement of Energetic Ions in the Plasma Sheet

[9] The Geotail satellite was placed in the near-Earth orbit of ~9 × 30 R_E in the fall of 1994 [*Nishida*, 1994] and surveys the near-Earth and midtail plasma sheet frequently. Geotail is equipped with the EPIC instrument which provides mass and charge state information about ions with an energy/charge range of 9 keV/*e* to 210 keV/*e* in eight spectral points [*Williams et al.*, 1994]. The instrument has a spatial coverage of almost 4π sr with six identical telescopes having a field of view of ±(0°–26.7°), ±(26.7°–53.3°), and ±(53.3°–80.0°) in elevation with respect to the spacecraft spin plane. It takes ~24 s to get one complete energy spectrum for H^+ ions, and ~48 s for O^+ ions. From each energy spectrum we calculated energy density (ε) of H^+ and O^+ by the following equation:

$$\varepsilon = \sqrt{2m}\,\pi \sum_{i=1}^{8} \sum_{j=1}^{6} \sqrt{E_i}\,\hat{J}(E_i, \theta_j) \cos\theta_j \Delta E_i \Delta\theta_j, \qquad (1)$$

where m is ion mass, E_i (ΔE_i) is the center energy (the energy band width) of the ith energy step, θ_j ($\Delta\theta_j$) is the elevation

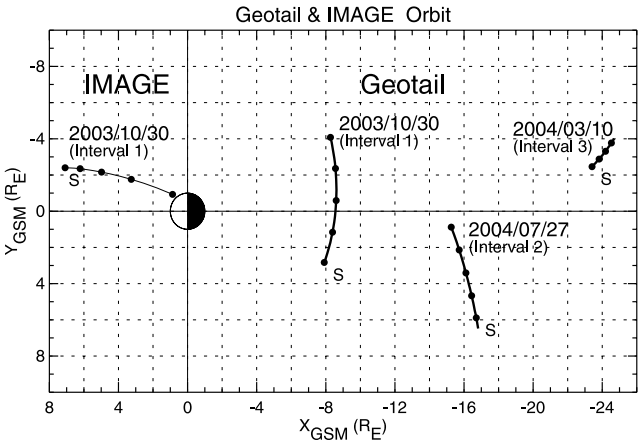

Figure 1. Orbits of the IMAGE satellite (thin line) and the Geotail satellite (thick lines) projected in the equatorial plane. The "S" characters denote the start of the orbital segments for the interval, and dots show the satellite locations at integer hour.

angle (angular coverage in elevation angle) of the jth polar sector, and $\hat{J}$ is the spin-averaged differential flux [*Nosé et al.*, 2001, 2003]. For statistical significance, we took an average of energy density over 5 min, which is used in the following analysis to examine temporal changes of ion composition in the plasma sheet. We also used the magnetic field data obtained by the magnetic field (MGF) instrument [*Kokubun et al.*, 1994] onboard the Geotail satellite.

3. Event Selection

[10] From the period of August 2003 through July 2004, we selected time intervals during which IMAGE/LENA or FAST/IESA made an observation of ions of ionospheric origin simultaneously with Geotail/EPIC. The selection criteria are as follows: (1) geomagnetic storms took place; (2) the Geotail satellite mostly stayed in the nightside plasma sheet; and (3) clear substorm signatures were identified by ground stations and geosynchronous satellites during the magnetic storm. These selection criteria yielded 3 time intervals, that is, 1900–2300 UT on 30 October 2003 (interval 1), 0130–0600 UT on 27 July 2004 (interval 2), and 0400–0730 UT on 10 March 2004 (interval 3). In interval 1, both IMAGE/LENA and Geotail/EPIC data were available. Intervals 2 and 3 are conjunction observations by FAST/IESA and Geotail/EPIC. Figure 1 shows orbits of the satellites in the X-Y plane in GSM (Geocentric Solar Magnetospheric) coordinates for these 3 intervals. Thin line on the dayside indicates the IMAGE orbit for interval 1 and thick lines at $X_{GSM} < -8\ R_E$ indicate the Geotail orbits. Characters "S" denote start of the satellite orbit during the selected intervals and dots on orbits show the locations of the satellite at integer hour. Geotail flew at $X_{GSM} \sim -8$, -16, and $-24\ R_E$ in the interval 1, 2, and 3, respectively.

4. Observation and Analysis

4.1. Interval 1 (1900–2300 UT on 30 October 2003)

[11] This interval is in the main phase of the October 2003 superstorm. Overall features of O^+ ions during this superstorm has been discussed by *Nosé et al.* [2005], but the present study focuses on O^+ ion dynamics in the course of storm time substorms as shown later in Figures 4 and 11.

[12] Figure 2 (top) shows the SYM-H index decreasing from −150 nT to −400 nT during the time interval of 1900–2300 UT on 30 October 2003. Figure 2 (bottom) displays the energetic (105–150 keV and 225–315 keV) electron flux from the LANL-01A geosynchronous satellite as well as the X component of the geomagnetic field at Lerwick (LER, 62.0° geomagnetic latitude (GMLAT), 89.0° geomagnetic longitude (GMLON)) and Narsarsuaq (NAQ, 70.0° GMLAT, 38.6° GMLON). The first substorm was identified at 1947 UT by energetic electron flux enhancement at the geosynchronous satellite and high-latitude negative bays at both LER and NAQ, as indicated by a vertical dashed line. We found another substorm onset at 2115 UT which is also indicated by a vertical dashed line; this substorm is characterized by energetic electron flux enhancement and high-latitude negative bay at LER.

[13] Figures 3a and 3b show the LENA images around the Earth obtained by the IMAGE satellite before and after the first substorm onset (1947 UT), respectively. The perspective

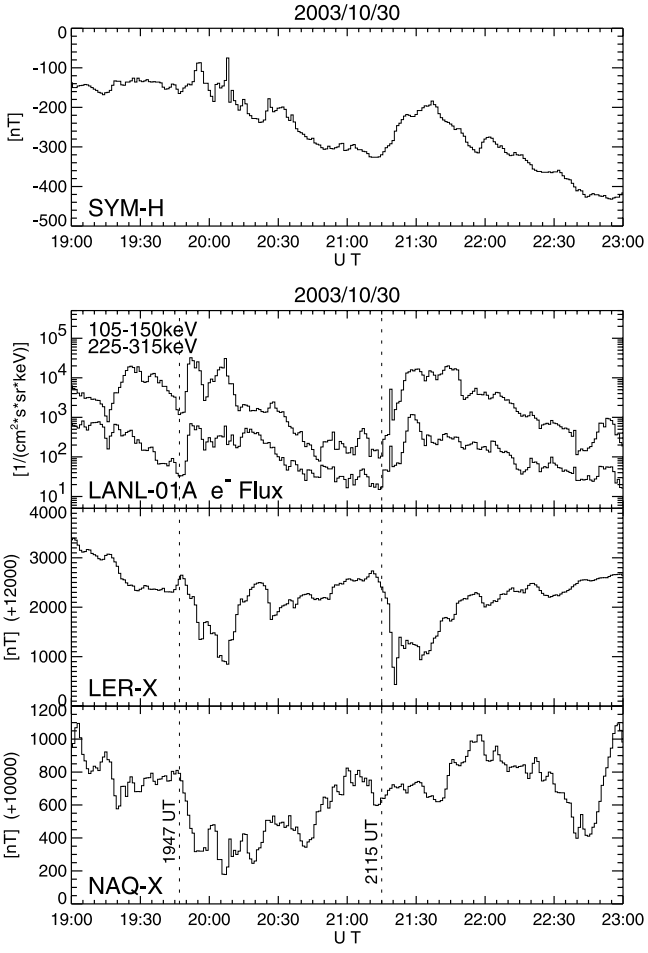

Figure 2. (top) The SYM-H index for 1900–2300 UT on 30 October 2003 (interval 1). (bottom) The energetic electron flux from the LANL-01A geosynchronous satellite as well as the X component of the geomagnetic field at Lerwick (LER, 62.0° GMLAT) and Narsarsuaq (NAQ, 70.0° GMLAT). Substorm onsets were identified at 1947 UT and 2115 UT.

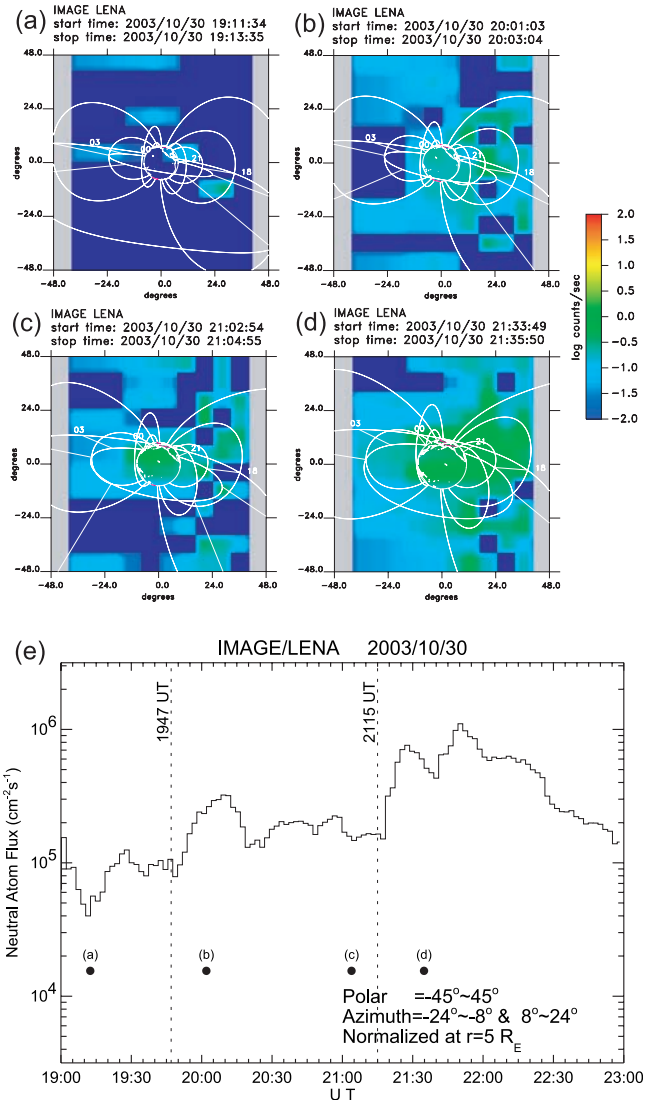

Figure 3. (a) The neutral atom flux around the Earth from the LENA imager before the 1947 UT substorm in interval 1. The Earth is at the center, and the magnetic field lines at noon, dusk, midnight, and dawn are shown for $L = 3$ and $L = 5$. (b) The LENA image after the 1947 UT substorm. (c and d) The LENA image before and after the 2115 UT substorm. (e) The neutral atom flux averaged over the polar angle of ±45° (x direction of the image) and the azimuthal angle of ±24° (y direction of the image) with the exclusion of the equatorial area (i.e., the azimuthal angle of −8° to 8°). The flux is normalized as it is measured at $r = 5\ R_E$. Black circles indicate times when the LENA images of Figures 3a–3d were taken.

view is from the dayside where the IMAGE satellite was located. The magnetic field lines at 0000, 0600, 1200, and 1800 magnetic local time (MLT) are drawn for L value of 3 and 5 with while lines. Comparing Figures 3a and 3b, we found that low-energy neutral atom flux coming from the direction of the Earth was enhanced after the substorm. Figures 3c and 3d show LENA images before and after the second substorm onset (2115 UT). We also found strong flux enhancement of neutral atoms after this substorm onset. It is worthwhile to briefly mention that it is difficult to identify the source region of outflowing flux (i.e., auroral zone, cusp, or polar cap), because the observed neutral atom flux is a result of integration of flux along the line of sight. Nevertheless, we suppose that the outflowing flux predominantly originates from the auroral zone, as seen later in intervals 2 and 3 (Figures 6 and 9). In order to see temporal changes of the low-energy neutral atom flux in more detail, we averaged the neutral atom flux around the Earth over the polar angle of ±45° (x direction of the image) and the azimuthal angle of ±24° (y direction of the image) with exclusion of the equatorial area (i.e., the azimuthal angle of −8° to 8°). Then we computed the normalized flux ($J_{\text{normalized}}$) from the average flux derived above (J_{averaged}) as it is measured at radial distance of 5 R_E, by

$$J_{\text{normalized}} = J_{\text{averaged}} \times \left(\frac{r - 1.5}{5 - 1.5}\right)^2, \qquad (2)$$

where r is the radial distance of the satellite position in R_E. Here the neutral atom source was assumed to be at geocentric altitude of 1.5 R_E [*Khan et al.*, 2003]. This generates time series data of neutral atom flux around the Earth with a time resolution of 2 min. We calculated a running average of $J_{\text{normalized}}$ with a time window of 8 min, which is displayed in Figure 3e. Vertical dashed lines indicate onset time of the substorms. Black circles corresponds to times in which the LENA images of Figures 3a–3d were taken. We found that the neutral atom flux started to increase with a short delay (∼5 min) to the substorm onsets. It should be noted that this time delay includes travel time of low-energy neutral atoms from their source site to the IMAGE satellite, because it takes about 1.5–2/6–7 min at least for 500 eV hydrogen/oxygen atoms to travel from $r = 1.5\ R_E$ (the source site where charge exchange occurs) to $r = 6$–$7\ R_E$ (the IMAGE position). Thus the ionospheric ion outflow is considered to respond almost immediately (within several minutes) to the substorms. At the first substorm the neutral atom flux was enhanced from 1×10^5 cm^{-2} s^{-1} to 3×10^5 cm^{-2} s^{-1} within 20 min. The second substorm was accompanied by a sudden increase of the neutral atom flux from 2×10^5 cm^{-2} s^{-1} to 1×10^6 cm^{-2} s^{-1}. These results indicate that the substorms caused an enhancement of outflowing ion flux by a factor of 3–5.

[14] Figure 4 shows the magnetic field in the X_{GSM} and Z_{GSM} components and the O^+/H^+ energy density ratio measured by the Geotail satellite which was located at $X_{GSM} \sim -8\ R_E$ (Figure 1). Two vertical lines indicate onset time of the substorms (1947 UT and 2115 UT). At the first substorm onset, the absolute value of B_x decreased and B_z increased, indicating that dipolarization took place. At the same time the O^+/H^+ energy density ratio increased suddenly from ∼1 to 3 within 10 min, and then it showed a gradual increase during 2000–2030 UT, even though the substorm expansion phase ended around 2010 UT as can be seen in B_z changes. For the second substorm onset, signatures of the magnetic field and the O^+/H^+ energy density ratio were similar to those of the first substorm; that is, the magnetic field was dipolarized and the energy density ratio increased rapidly at substorm onset, followed by a gradual increase with a time scale of 1 h (2130–2230 UT).

4.2. Interval 2 (0130–0600 UT on 27 July 2004)

[15] In Figure 5 we plotted the SYM-H index, the elevation angle of the magnetic field observed by the GOES 10 sat-

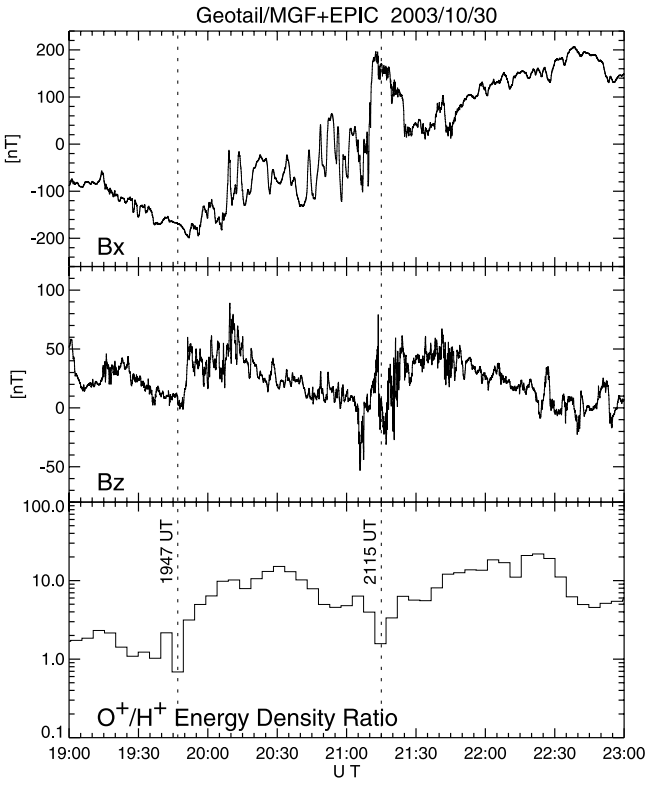

Figure 4. The (top) X and (middle) Z components of the magnetic field measured by Geotail/MGF and (bottom) the O^+/H^+ energy density ratio from Geotail/EPIC/STICS for 1900–2300 UT on 30 October 2003 (interval 1).

ellite, the energetic (50–75 keV and 75–105 keV) electron flux from the LANL-01A satellite, and the X component of the geomagnetic field at Glenlea (GLN, 58.6° GMLAT, 327.8° GMLON). This interval was in the main phase of a strong magnetic storm and the SYM-H index was changing between −50 nT and −150 nT. At 0214 UT we found increases of the magnetic field elevation angle (i.e., dipolarization) and energetic electron flux at geosynchronous orbit, indicating substorm occurrence. Another substorm onset was identified at 0357 UT by dipolarization at GOES 10, energetic electron flux enhancement at LANL-01A, and a high-latitude negative bay at GLN.

[16] Figures 6a and 6b show the FAST/IESA data around the onset time of the two substorms (0214 UT and 0357 UT). Figures 6a and 6b (top) display the E-t diagram and Figures 6a and 6b (bottom) show the ion flux integrated over the energy range of 50–1000 eV and pitch angle of 90°–270°. The FAST satellite was in the northern hemisphere in these time intervals, thus these ions can be considered to be outflowing from the ionosphere to the magnetosphere. (Ions with pitch angle of 180° are flowing upward along the magnetic field.) From Figure 6a we notice that the FAST satellite was in the auroral zone before the substorm onset (i.e., 0214 UT) and observed outflowing ion flux of $\sim 2 \times 10^7$ cm^{-2} s^{-1}. At 0215 UT the substorm onset caused a prompt increase of the ion flux which reached a peak value of $\sim 10^9$ cm^{-2} s^{-1}. Figure 6b also indicates that the FAST satellite traversed over the auroral zone during the second substorm. The observed flux just before 0357 UT was $\sim 5 \times 10^6$ cm^{-2} s^{-1}, whereas it increased to an order of 10^8–10^9 cm^{-2} s^{-1} after 0357:35 UT. These results suggest that the outflowing ion flux increased by a factor of 20–50 almost simultaneously ($\lesssim$1 min) with the substorm onset.

[17] Figure 7 shows the Geotail observations of the magnetic field and ion composition at $X \sim -16\ R_E$ in the same format as Figure 4. Two vertical lines represent substorm onset time (0214 UT and 0357 UT). At the first substorm onset, there is no clear dipolarization signatures in the magnetic field. We suppose that this is because the substorm onset region was localized and the Geotail satellite was far from there. Because of lack of substorm signature at the Geotail position, there seems no sudden increases in the O^+/H^+ energy density ratio. However, after the substorm onset the O^+/H^+ energy density ratio showed gradual increase with a time scale of 1 h (0230–0330 UT), as the same case of substorms in interval 1 (Figure 4). When the second substorm took place at 0357 UT, no clear substorm signatures were also

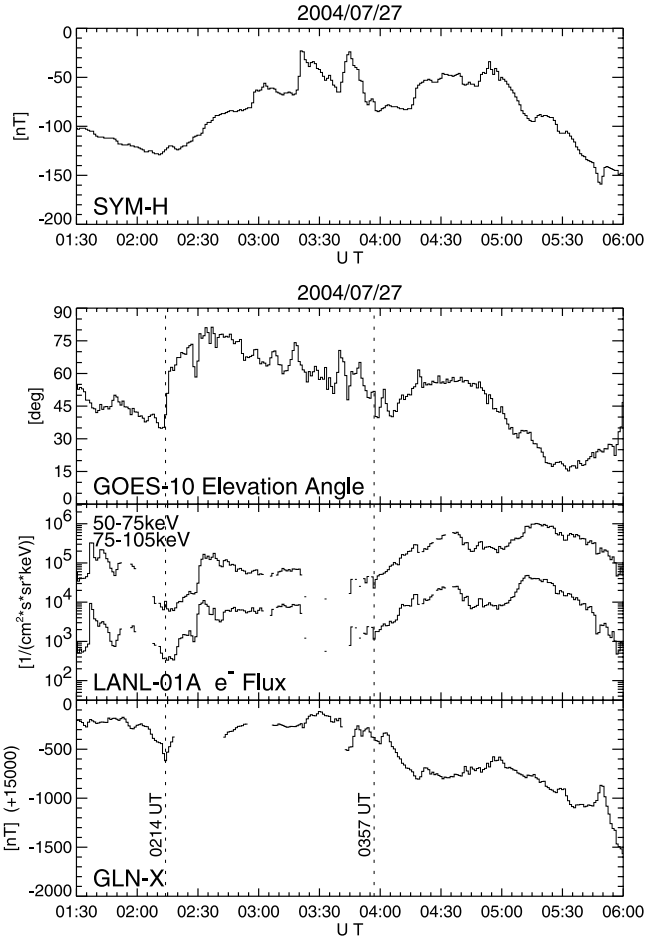

Figure 5. (top) The SYM-H index for 0130–0600 UT on 27 July 2004 (interval 2). (bottom) The elevation angle of the magnetic field measured by the GOES 10 geosynchronous satellite, the energetic electron flux from the LANL-01A geosynchronous satellite, and the X component of the geomagnetic field at Glenlea (GLN, 58.6° GMLAT). Substorm onsets were identified at 0214 UT and 0357 UT.

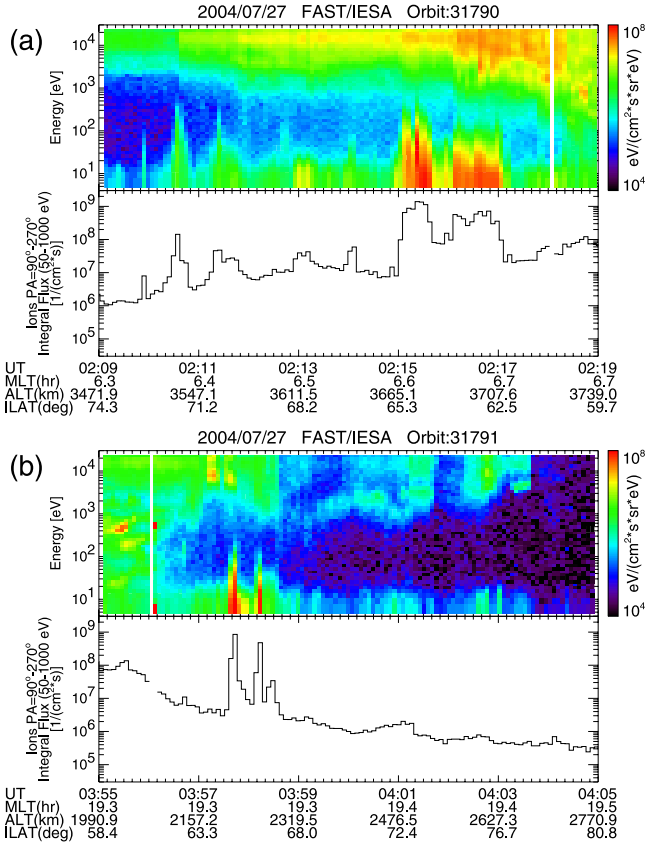

Figure 6. (a) The ion flux from FAST/IESA around the 0214 UT substorm in interval 2: (top) the E-t diagram and (bottom) the ion flux integrated over energy range of 50–1000 eV and pitch angle of 90°–270°. (b) The FAST/IESA data around the 0357 UT substorm in interval 2. Format is the same as Figure 6a.

observed by Geotail in the magnetic field. About 45 min after the substorm onset (around 0450 UT), however, fluctuation of the magnetic field was enhanced in both B_x and B_z; the absolute value of B_x decreased and B_z showed a small increase. We suggest that these are possible signatures of local dipolarization. The 45 min delay may be explained by the longitudinal and radial expansion of local dipolarization region [e.g., *Nagai*, 1982; *Jacquey et al.*, 1991]. The local dipolarization at ~0450 UT was accompanied by a sudden enhancement of the O^+/H^+ energy density ratio. The magnetic field implies that the local dipolarization ceased with 15 min, though the O^+/H^+ energy density ratio stayed at almost constant level for ~40 min.

4.3. Interval 3 (0400–0730 UT on 10 March 2004)

[18] Figure 8 compiles the SYM-H index, the elevation angle of the magnetic field observed by the GOES 10 satellite, the energetic (75–113 keV and 113–170 keV) proton flux from the LANL-02A satellite, and the X component of the geomagnetic field at Baker Lake (BLC, 73.2° GMLAT, 322.0° GMLON). This interval was found near the peak of a moderate magnetic storm and the SYM-H index was between −60 nT and −100 nT. We identified occurrence of a substorm at 0528 UT by dipolarization and energetic proton flux enhancement at geosynchronous satellites, and a negative bay at high-latitude ground station.

[19] Figure 9 displays the FAST/IESA data during the substorm of 0528 UT in the same format as Figure 6. At 0528 UT invariant latitude of the FAST satellite was 74°–75° and there are little fluxes in the E-t diagram, indicating that the satellite was in the polar cap. Although a sudden increase of outflowing ion flux (~3×10^8 cm^{-2} s^{-1}) can be seen at 0529:55 UT, this enhancement may be caused not by temporal effects due to substorm onset but by spatial effects due to satellite motion to the auroral zone. Around 0531–0532 UT the FAST satellite is considered to be flying over the auroral zone and observed flux of ~5×10^6 cm^{-2} s^{-1}. The outflowing flux is enhanced again at 0532:30 UT and reached the almost same level as the previous enhancement at 0529:55–0530:45 UT. We suggest that these flux enhancements at two different latitude are caused by formation of a double auroral arc at the substorm onset. Since the first enhancement of outflowing flux was observed at 0529:55 UT, we can expect that ion outflow responded to the substorm before that time. This idea leads us to conclude that the delay time of ion outflow from the substorm onset was <2 min. Enhancement factor is estimated as ~50 (i.e., ~5×10^6 cm^{-2} s^{-1} to ~3×10^8 cm^{-2} s^{-1}).

[20] Figure 10 demonstrates the Geotail data at $X \sim -24$ R_E in the same format as Figure 4. At the substorm, which is indicated by a vertical line, the absolute value of B_x decreased and B_z increased, being a dipolarization signature. For about 1 h prior to the substorm onset (i.e., 0430–0528 UT), Geotail was in the magnetic lobe and we could not

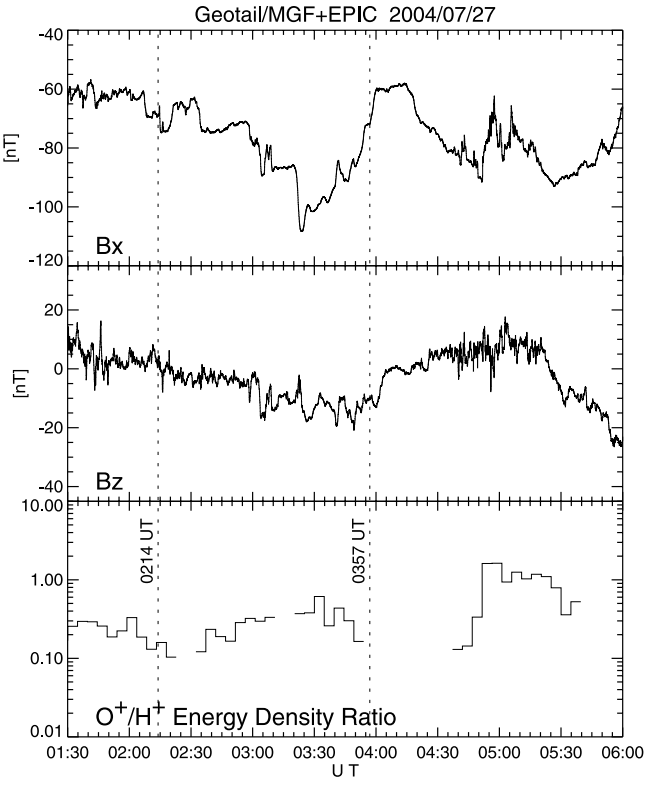

Figure 7. The magnetic field and the O^+/H^+ energy density ratio data for interval 2. Format is the same as Figure 4.

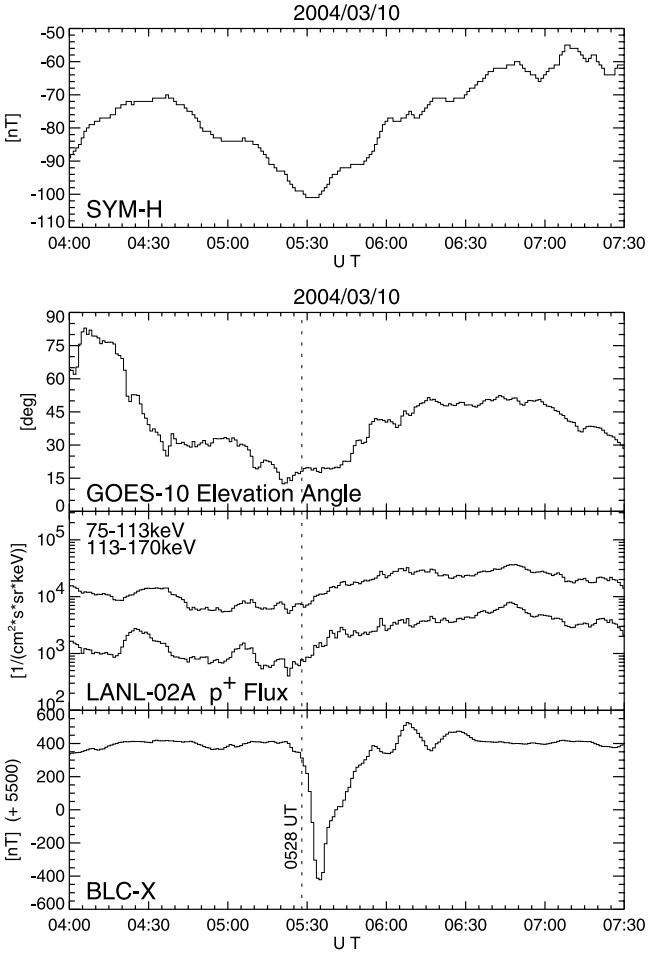

Figure 8. (top) The SYM-H index for 0400–0730 UT on 10 March 2004 (interval 3). (bottom) The elevation angle of the magnetic field measured by the GOES 10 geosynchronous satellite, the energetic proton flux from the LANL-02A geosynchronous satellite, and the X component of the geomagnetic field at Baker Lake (BLC, 73.2° GMLAT). Substorm onset was identified at 0528 UT.

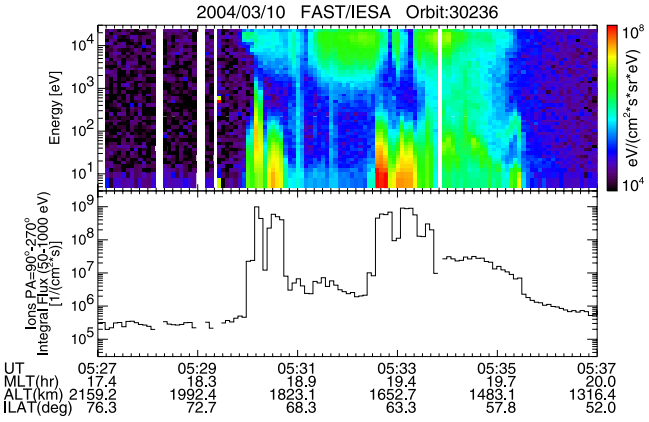

Figure 9. The ion flux from FAST/IESA for interval 3. Format is the same as Figure 6.

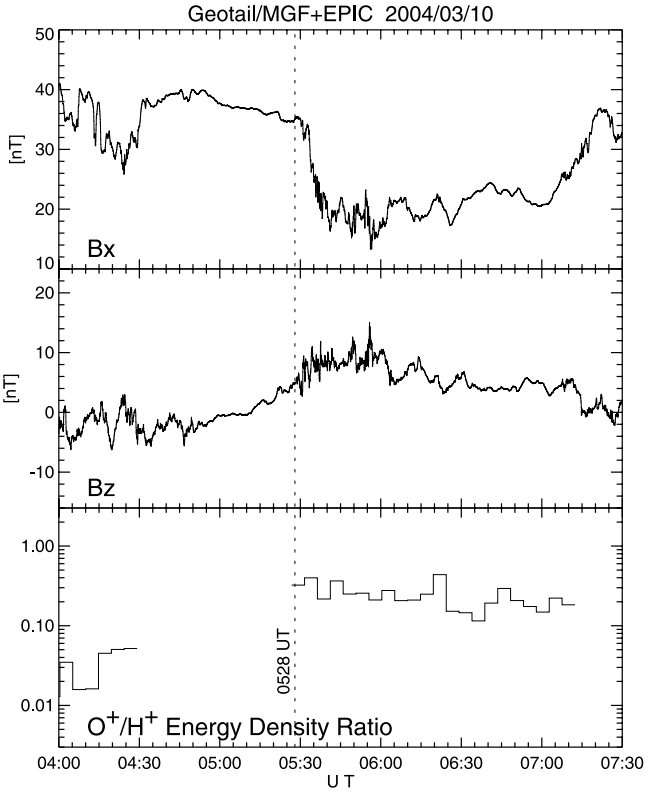

Figure 10. The magnetic field and the O^+/H^+ energy density ratio data for interval 3. Format is the same as Figure 4.

calculate the energy density ratio in the plasma sheet. However, before 0430 UT the satellite made a measurement of energetic ion flux in the plasma sheet, which indicates the O^+/H^+ ratio of 0.02–0.05. Assuming that the O^+/H^+ energy density ratio did not change significantly before the substorm onset, we can expect that the energy density ratio was strongly enhanced at dipolarization. Even though the substorm expansion phase has ended around 0550–0600 UT as can be noted from the magnetic field data, the O^+/H^+ energy density ratio stayed at almost constant level of 0.2–0.3 for about 1 h.

5. Discussion

5.1. Response of Outflowing Ion Flux to Substorms

5.1.1. Enhancement Factor

[21] The IMAGE/LENA and FAST/IESA observations revealed that substorms can cause drastic changes of the ion flux outflowing from the Earth by a factor of 3–50 (Figures 3, 6, and 9). This flux change related to substorms is comparable to or larger than that during Kp increase from 0 to 6 (i.e., fivefold to tenfold) which was statistically revealed by *Yau et al.* [1988], *Abe et al.* [1996], and *Cully et al.* [2003b]. Thus it is important to take substorm effects into consideration when we study outflowing ion flux. It is expected that such drastic change of outflowing ion flux at substorms possibly affects ion composition in the plasma sheet; this issue will be discussed in section 5.2.

[22] Here we briefly compare our observational results (a factor of 3–50) with that by *Wilson et al.* [2004]; that is, the ion outflow rate at the nightside auroral zone increases

by only a factor of ~2 after onset. The discrepancy of the outflow flux change may be due to different approaches in data analysis. The present study examined temporal changes of the outflow flux for 3 individual intervals during magnetic storms, while *Wilson et al.* [2004] conducted the superposed epoch analysis which makes drastic flux changes smooth. The approach by Wilson et al. will lower the enhancement factor of the outflow flux to be estimated.

5.1.2. Response Time

[23] From analysis of the 3 intervals including substorm onsets, we found that the ion outflow responded to storm time substorms within several minutes (Figures 3, 6, and 9). It is noteworthy to mention that the two substorms in interval 1 appeared to be associated with strong compression of the magnetosphere during high solar wind dynamic pressure, as discussed by *Nosé et al.* [2005]. At the substorm onset in interval 3 there was a weak dynamic pressure enhancement (from 5.5 nPa to 6.5 nPa) which is due to slight solar wind velocity enhancement (from 650 km/s to 700 km/s), according to the ACE measurements (not shown here). On the other hand, the ACE satellite observed no clear changes in the solar wind dynamic pressure around the substorms in interval 2, but rather northward turnings of the IMF with amplitudes of 10–20 nT (not shown here).

[24] Recent studies by *Fuselier et al.* [2002], *Khan et al.* [2003], and *Kunori et al.* [2007] reported that enhancements of solar wind dynamic pressure led to bursts of ion outflow. *Fuselier et al.* [2002] examined the 24 June 2000 ion outflow event and found that both auroral emission and the ion outflow increased on the duskside (18–19 MLT) at pulses of the solar and dynamic pressure. Analyzing the same ion outflow event, *Khan et al.* [2003] revealed that the delay time between the solar wind dynamic pressure and ion outflow response was ~2 min. From 3-D multifluid simulations of the 29 October 2003 storm, *Harnett et al.* [2008] showed that variations of IMF B_y and B_z caused prompt increase of ionospheric outflows. Since substorms are triggered preferentially by the enhancement of the solar wind dynamic pressure [e.g., *Kokubun et al.*, 1977] or by the changes of the IMF direction [e.g., *Lyons et al.*, 1997], our results are consistent with these previous results; moreover we suppose that substorms play a more direct role rather than solar wind variations in enhancement of outflowing ion flux.

[25] The generating process of outflowing ions is well documented by *Strangeway et al.* [2005]. They considered two primary energy sources of ion outflow: downward Poynting flux and soft electron precipitation, both of which are expected to appear at substorm onsets. The downward Poynting flux would cause the ion upwelling via the Joule dissipation at the lower ionosphere, while the soft electron precipitation would cause the ion upwelling through the ambipolar electric field which accompanies with ionospheric electron heating at high altitudes. The upwelling ions should be further accelerated by transverse electromagnetic waves to escape from the ionosphere. The above multistep processes may be activated within several minutes after substorm onset. In actuality, the EISCAT Tromso radar observed about 4 min of delay between auroral breakup and increase of upward ion velocity, which is generated by the soft electron precipitation, when a shock-triggered substorm occurred at 2024 UT on 25 September 2001 (Y. Ogawa, private communication, 2008). This time delay is slightly longer but close to our observations, if the acceleration of upwelling ions to flow out from the ionosphere takes place quickly.

5.2. Ion Composition Change in Plasma Sheet

5.2.1. Two-Step Effect of Substorms

[26] Geotail observation of the O^+/H^+ energy density ratio in the plasma sheet showed the first sudden enhancement at local dipolarization and the subsequent gradual increase (Figures 4, 7, and 10). We consider that the first sudden enhancement is caused by mass-dependent acceleration of preexisting ions at dipolarization and the subsequent gradual increase is due to an additional supply of O^+ ions which are extracted from the ionosphere at the substorm onset. This idea is supported by energy spectral changes during the course of substorms observed by the Geotail/EPIC instrument. The top two plots of Figure 11 display the H^+ and O^+ energy spectra in the plasma sheet for the substorm onset at 1947 UT on 30 October 2003. Likewise, the subsequent pairs of plots show the H^+ and O^+ energy spectra for 4 other substorms (the second substorm in interval 1, two substorms in interval 2, and a substorm in interval 3). Different colors correspond to different time intervals; that is, green, yellow, and red lines represent energy spectra before onset, 5–15 min after onset (local dipolarization), and 30–60 min after onset (local dipolarization), respectively. Note that in the third pair of plots the energy spectra just after the onset (yellow line) are not drawn because local dipolarization signature was not observed (Figure 7).

[27] It was found that the H^+ energy spectra did not show significant changes in all substorm onsets. However, the O^+ energy spectra changed drastically at the energy range of a few tens of keV to 100 keV and became harder after dipolarization (yellow line), implying that acceleration of ions was more effective to O^+ ions than H^+ ions. Such mass-dependent acceleration of ions has been reported by numerical simulation [*Delcourt et al.*, 1990; *Sánchez et al.*, 1993] as well as by satellite observation [*Nosé et al.*, 2000]. When an inductive electric field associated with the local dipolarization has a time scale comparable to the O^+ gyroperiod (and therefore longer than the H^+ gyroperiod), the first adiabatic invariant of O^+ ions is violated and they can be accelerated nonadiabatically. However, H^+ ions primarily undergo $E \times B$ drift and gain little additional energy.

[28] At 30–60 min after the onset, we found that O^+ flux in lower energy range from 9 keV to a few tens of keV showed a further increase (red line), resulting in a softer energy spectrum. From the spectral shape we can surmise that the O^+ flux of $\leq$9 keV became higher at 30–60 min after the onset (red line) than before the onset (green line) and at 5–15 min after the onset (yellow line). The O^+ increase in the lower energy range can be explained by that extra O^+ ions are transported into the plasma sheet within 30–60 min after they are extracted from the ionosphere at substorm onset as observed by the LENA imager and the IESA instruments (Figures 3, 6, and 9). This explanation is supported by a number of previous studies which examined trajectories of ionospheric ions originated from the nightside auroral zone. [*Chappell et al.*, 1987] argued that the auroral zone supplies almost 50% of O^+ ions of the plasma sheet. *Peroomian and Ashour-Abdalla* [1996] calculated ion trajectories in the

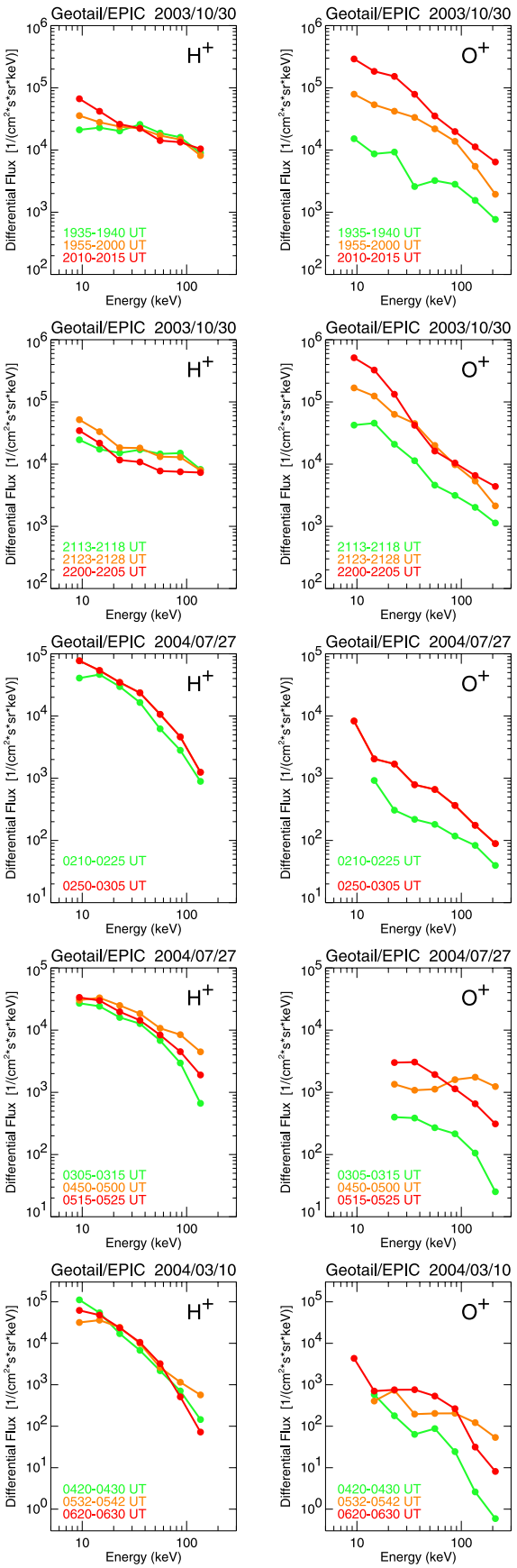

terrestrial electric and magnetic field models during slightly disturbed times (Kp = 1–2) and showed that the nightside auroral zone is the dominant source of O^+ ions in the near-Earth tail ($X \geq -20\ R_E$ to $-30\ R_E$). [*Delcourt et al.*, 1999] also performed a test particle simulation for upflowing 100 eV O^+ ions near the poleward boundary of the auroral oval and found that they are convected to the near-Earth plasma sheet ($X \sim -9\ R_E$ to $-10\ R_E$). The similar results were reported by other particle-tracing studies [e.g., *Chappell et al.*, 2000; *Huddleston et al.*, 2005; *Moore et al.*, 2005; *Harnett et al.*, 2008]. The transit time of ions from the ionosphere to the plasma sheet is estimated to be $\leq$1–2 h by some of the aforementioned studies, which is consistent with our observational results.

[29] The present coordinated observations by IMAGE/LENA, FAST/IESA, and Geotail/EPIC revealed that substorms have both an immediate effect and a delayed effect on the ion composition in the plasma sheet, which are also reported by recent numerical simulations [*Fok et al.*, 2006; *Moore et al.*, 2007]. We suppose that the two-step effect of substorms is rather common over a wide area of the plasma sheet, because the Geotail observations were similar at three different locations ($X_{GSM} \sim -8$, -16, and $-24\ R_E$).

5.2.2. Comparison With Previous Studies

[30] Some previous studies investigated ion composition change in the plasma sheet when substorms were initiated. Using the CRRES/MICS instrument which covers the energy range from several tens of keV to 400 keV, *Grande et al.* [1999] and *Daglis et al.* [2000] examined ion composition change at $L = 5–8$ during storm time substorms. *Grande et al.* [1999] showed that the O^+ count rate is increased at onset and stays at enhanced level for at least 45 min. The similar feature can be seen in the O^+ energy density in Figure 1 of *Daglis et al.* [2000]. These ion composition change have been interpreted as a result of prompt and direct feeding of ions from the ionosphere to the magnetosphere [e.g., *Daglis and Axford*, 1996]. At $X \sim -14.5\ R_E$, the AMPTE/IRM satellite observed that the differential flux of 160 keV O^+ ions was more pronounced than the differential flux of 160 keV H^+ ions at a substorm onset [*Möbius et al.*, 1987]. This event was considered as an indication of additional injection of ionospheric plasma from the near-Earth neutral line region to the plasma sheet after substorm onset. Further tailward, that is, at radial distance of $\sim$19 R_E, recent studies employing the Cluster/CODIF instrument showed that the O^+/H^+ pressure ratio increases at storm time substorms [*Kistler et al.*, 2005, 2006]. The increase of the pressure ratio was caused by a sudden loss of H^+ with a gradual decrease of the O^+ pressure. Kistler et al. supposed that both ions are transported away from the onset region but O^+ is then replenished quickly. It should be noted that the Cluster/CODIF instrument covers the energy range of 40 eV–40 keV which is lower than that of other studies. Different behavior of O^+ flux (i.e., gradual

Figure 11. Geotail observations of energy spectra of (left) H^+ ion and (right) O^+ ion during the course of substorm. Different colors represent different time intervals: green, yellow, and red show energy spectra before onset, 5–15 min after onset (local dipolarization), and 30–60 min after onset (local dipolarization), respectively. The five pairs of plots correspond to five examined substorm onsets.

decrease after onsets) may be due to the different energy range. In the distant tail of $X = -40\ R_E$ to $-66\ R_E$, energetic (144 keV–4 MeV) O^+ bursts were observed after substorm onset by the Geotail/HEP-LD instrument [*Zong et al.*, 1998]. These O^+ ions were thought to leave the polar ionosphere at the substorm onset and be transported to the distant tail where ion acceleration took place.

[31] All of these previous studies described that the O^+ flux (or the O^+/H^+ ratio) increased after substorm onset and O^+ ions were considered to be extracted from the ionosphere at the onset. This feature was identified in a wide range of distance spanning from the magnetosphere/the near-Earth plasma sheet ($L = 5–8$) to the distant tail ($X \sim -66\ R_E$). These results are well consistent with the present observational results by IMAGE/LENA, FAST/IESA, and Geotail/EPIC.

6. Summary

[32] We examined variations of ions of ionospheric origin over the ionosphere and in the plasma sheet when storm time substorms were initiated. From the IMAGE/LENA and FAST/IESA observations we found that the outflowing ion flux from the ionosphere was enhanced by a factor of 3–50 at substorms. This factor is comparable to or larger than the factor which was statistically found by previous studies between quiet condition (Kp = 0) and disturbed condition (Kp = 6). This indicates that effect of substorm to the ion outflow is not negligible. The ionospheric ion outflow is suggested to respond to the substorm onset within several minutes. This time delay is considered to be due to activation time of the multiprocess including ion upwelling in the ionosphere and additional acceleration to escape from the ionosphere.

[33] The Geotail/EPIC observation showed that the O^+/H^+ energy density ratio in the plasma sheet was immediately enhanced when local dipolarization signatures appeared, and then increased gradually or stayed at nearly constant level in a time scale of 1 h even if substorm expansion phase has ended. These Geotail observations were similar among three different locations of $X_{GSM} \sim -8$, -16, and $-24\ R_E$. The first sudden increase of the O^+/H^+ energy density ratio is considered as a result of mass-dependent acceleration at dipolarization. The following gradual increases are supposed to be due to an additional supply of O^+ ions from the ionosphere which were outflowing at substorm onset, as observed by IMAGE/LENA and FAST/IESA. The above idea was supported by the energy spectral changes of H^+ and O^+ ions in the plasma sheet. We conclude that substorms play a two-step role in changes of the plasma sheet ion composition.

[34] **Acknowledgments.** We thank D. J. Williams, R. W. McEntire, A. T. Y. Lui, and S. R. Nylund for their help in processing the Geotail/EPIC data. We also thank T. Nagai for providing the Geotail/MGF data. The geomagnetic field data from high-latitude stations (LER, NAQ, GLN, and BLC) were provided by institutes operating each station through INTERMAGNET and WDC for Geomagnetism, Kyoto. The SYM-H index was provided by T. Iyemori at WDC for Geomagnetism, Kyoto. The GOES 10 magnetic field data were provided by H. Singer through the NOAA/NGDC SPIDR (Space Physics Interactive Data Resource) Web site. The energetic particle data from the LANL geosynchronous satellites were provided by courtesy of G. Reeves and D. Belian. Thanks are due to K. Hosowaka, Y. Miyashita, Y. Ogawa, and A. Ieda for their helpful comments. This work was supported by the Kurata Memorial Hitachi Science and Technology Foundation (grant 844), the Japan Securities Scholarship Foundation (grant 1368), Inamori Foundation, and the Ministry of Education, Science, Sports and Culture, Grant-in-Aid for Young Scientists (B) (grants 17740327 and 19740303).

[35] Wolfgang Baumjohann thanks Dimitrios Sarafopoulos and another reviewer for their assistance in evaluating this paper.

References

Abe, T., S. Watanabe, B. A. Whalen, A. W. Yau, and E. Sagawa (1996), Observations of polar wind and thermal ion outflow by Akebono/SMS, *J. Geomagn. Geoelectr.*, *48*, 319–325.

Burch, J. L. (2000), Image mission overview, *Space Sci. Rev.*, *91*, 1–14.

Carlson, C. W., R. F. Pfaff, and J. G. Watzin (1998), The Fast Auroral SnapshoT (FAST) mission, *Geophys. Res. Lett.*, *25*(12), 2013–2016.

Carlson, C. W., J. P. McFadden, P. Turin, D. W. Curtis, and A. Magoncelli (2001), The electron and ion plasma experiment for FAST, *Space Sci. Rev.*, *98*, 33–66.

Chappell, C. R., T. E. Moore, and J. H. Waite Jr. (1987), The ionosphere as a fully adequate source of plasma for the Earth's magnetosphere, *J. Geophys. Res.*, *92*(A6), 5896–5910.

Chappell, C. R., B. L. Giles, T. E. Moore, D. C. Delcourt, P. D. Craven, and M. O. Chandler (2000), The adequacy of the ionospheric source in supplying magnetospheric plasma, *J. Atmos. Sol. Terr. Phys.*, *62*, 421–436.

Cully, C. M., E. F. Donovan, A. W. Yau, and H. J. Opgenoorth (2003a), Supply of thermal ionospheric ions to the central plasma sheet, *J. Geophys. Res.*, *108*(A2), 1092, doi:10.1029/2001JA009457.

Cully, C. M., E. F. Donovan, A. W. Yau, and G. G. Arkos (2003b), Akebono/Suprathermal Mass Spectrometer observations of low-energy ion outflow: Dependence on magnetic activity and solar wind conditions, *J. Geophys. Res.*, *108*(A2), 1093, doi:10.1029/2001JA009200.

Daglis, I. A., and W. I. Axford (1996), Fast ionospheric response to enhanced activity in geospace: Ion feeding of the inner magnetotail, *J. Geophys. Res.*, *101*(A3), 5047–5065.

Daglis, I. A., Y. Kamide, C. Mouikis, G. D. Reeves, E. T. Sarris, K. Shiokawa, and B. Wilken (2000), "Fine structure" of the storm-substorm relationship: Ion injections during Dst decrease, *Adv. Space Res.*, *25*(12), 2369–2372.

Delcourt, D. C., J. A. Sauvard, and A. Pedersen (1990), Dynamics of single-particle orbits during substorm expansion phase, *J. Geophys. Res.*, *95*(A12), 20,853–20,865.

Delcourt, D. C., N. Dubouloz, J.-A. Sauvard, and M. Malingre (1999), On the origin of sporadic keV ion injections observed by Interball-Auroral during the expansion phase of a substorm, *J. Geophys. Res.*, *104*, 24,929–24,937.

Fok, M.-C., T. E. Moore, P. C. Brandt, D. C. Delcourt, S. P. Slinker, and J. A. Fedder (2006), Impulsive enhancements of oxygen ions during substorms, *J. Geophys. Res.*, *111*, A10222, doi:10.1029/2006JA011839.

Fuselier, S. A., H. L. Collin, A. G. Ghielmetti, E. S. Claflin, T. E. Moore, M. R. Collier, H. Frey, and S. B. Mende (2002), Localized ion outflow in response to a solar wind pressure pulse, *J. Geophys. Res.*, *107*(A8), 1203, doi:10.1029/2001JA000297.

Ghielmetti, A. G., R. G. Johnson, R. D. Sharp, and E. G. Shelley (1978), The latitudinal, diurnal, and altitudinal distributions of upward flowing energetic ions of ionospheric origin, *Geophys. Res. Lett.*, *5*(1), 59–62.

Gorney, D. J., A. Clarke, D. Croley, J. Fennell, J. Luhmann, and P. Mizera (1981), The distribution of ion beams and conics below 8000 km, *J. Geophys. Res.*, *86*(A1), 83–89.

Grande, M., C. H. Perry, A. Hall, J. Fennell, and B. Wilken (1999), Statistics substorm occurrence in storm and non-storm periods, *Phys. Chem. Earth Part C*, *24*(1–3), 167–172.

Harnett, E. M., R. M. Winglee, A. Stickle, and G. Lu (2008), Prompt ionospheric/magnetospheric responses 29 October 2003 Halloween storm: Outflow and energization, *J. Geophys. Res.*, *113*, A06209, doi:10.1029/2007JA012810.

Huddleston, M. M., C. R. Chappell, D. C. Delcourt, T. E. Moore, B. L. Giles, and M. O. Chandler (2005), An examination of the process and magnitude of ionospheric plasma supply to the magnetosphere, *J. Geophys. Res.*, *110*, A12202, doi:10.1029/2004JA010401.

Jacquey, C., J. A. Sauvaud, and J. Dandouras (1991), Location and propagation of the magnetotail current disruption during substorm expansion: Analysis and simulation of an ISEE multi-onset event, *Geophys. Res. Lett.*, *18*(3), 389–392.

Khan, H., M. R. Collier, and T. E. Moore (2003), Case study of solar wind pressure variations and neutral atom emissions observed by IMAGE/LENA, *J. Geophys. Res.*, *108*(A12), 1422, doi:10.1029/2003JA009977.

Kistler, L. M., et al. (2005), Contribution of nonadiabatic ions to the cross-tail current in an O^+ dominated thin current sheet, *J. Geophys. Res.*, *110*, A06213, doi:10.1029/2004JA010653.

Kistler, L. M., et al. (2006), Ion composition and pressure changes in storm time and nonstorm substorms in the vicinity of the near-Earth neutral line, *J. Geophys. Res.*, *111*, A11222, doi:10.1029/2006JA011939.

Kokubun, S., R. L. McPherron, and C. T. Russell (1977), Triggering of substorms by solar wind discontinuities, *J. Geophys. Res.*, *82*, 74–86.

Kokubun, S., T. Yamamoto, M. H. Acuna, K. Hayashi, K. Shiokawa, and H. Kawano (1994), The geotail magnetic field experiment, *J. Geomagn. Geoelectr.*, *46*, 7–21.

Kondo, T., B. A. Whalen, A. W. Yau, and W. K. Peterson (1990), Statistical analysis of upflowing ion beams and conic distributions at DE 1 altitudes, *J. Geophys. Res.*, *95*(A8), 12,091–12,102.

Kunori, T., M. Nosé, S. Taguchi, K. Hosokawa, M. R. Collier, and T. E. Moore (2007), Storm phase dependence of ion outflow: Statistical signatures obtained by IMAGE/LENA, *Geophys. Res. Lett.*, *34*, L18106, doi:10.1029/2007GL029877.

Lyons, L. R., G. T. Blanchard, J. C. Samson, R. P. Lepping, T. Yamamoto, and T. Moretto (1997), Coordinated observations demonstrating external substorm triggering, *J. Geophys. Res.*, *102*(A12), 27,039–27,051.

Möbius, E., M. Scholer, B. Klecker, D. Hovestadt, G. Gloeckler, and F. M. Ipavich (1987), Acceleration of ions of ionospheric origin in the plasma sheet during substorm activity, in *Magnetotail Physics*, edited by A. T. Y. Lui, pp. 231–234, Johns Hopkins Univ. Press, Baltimore, Md.

Moore, T. E. (1991), Origins of magnetospheric plasma, *Rev. Geophys.*, *29*, 1039–1048.

Moore, T. E., M. Lockwood, M. O. Chandler, J. H. Waite Jr., C. R. Chappell, A. Persoon, and M. Sugiura (1986), Upwelling O^+ ion source characteristics, *J. Geophys. Res.*, *91*(A6), 7019–7031.

Moore, T. E., et al. (2000), The low-energy neutral atom imager for IMAGE, *Space Sci. Rev.*, *91*, 155–195.

Moore, T. E., M.-C. Fok, S. P. Christon, S.-H. Chen, M. O. Chandler, D. C. Delcourt, J. Fedder, S. Slinker, and M. Liemohn (2005), Solar and ionospheric plasmas in the ring current region, in *Inner Magnetosphere Interactions: New Perspectives from Imaging*, *Geophys. Monogr. Ser.*, vol. 159, edited by J. Burch, M. Schulz, and H. Spence, pp. 179–194, AGU, Washington, D. C.

Moore, T. E., M.-C. Fok, D. C. Delcourt, S. P. Slinker, and J. A. Fedder (2007), Global aspects of solar wind-ionosphere interactions, *J. Atmos. Sol. Terr. Phys.*, *69*, 265–278.

Nagai, T. (1982), Observed magnetic substorm signatures at synchronous altitude, *J. Geophys. Res.*, *87*(A6), 4405–4417.

Nishida, A. (1994), The GEOTAIL mission, *Geophys. Res. Lett.*, *21*, 2871–2874.

Nosé, M., A. T. Y. Lui, S. Ohtani, B. H. Mauk, R. W. McEntire, D. J. Williams, T. Mukai, and K. Yumoto (2000), Acceleration of oxygen ions of ionospheric origin in the near-Earth magnetotail during substorms, *J. Geophys. Res.*, *105*(A4), 7669–7677.

Nosé, M., S. Ohtani, K. Takahashi, A. T. Y. Lui, R. W. McEntire, D. J. Williams, S. P. Christon, and K. Yumoto (2001), Ion composition of the near-Earth plasma sheet in storm and quiet intervals: Geotail/EPIC measurements, *J. Geophys. Res.*, *106*(A5), 8391–8403.

Nosé, M., R. W. McEntire, and S. P. Christon (2003), Change of the plasma sheet ion composition during magnetic storm development observed by the Geotail spacecraft, *J. Geophys. Res.*, *108*(A5), 1201, doi:10.1029/2004JA010930.

Nosé, M., S. Taguchi, K. Hosokawa, S. P. Christon, R. W. McEntire, T. E. Moore, and M. R. Collier (2005), Overwhelming O^+ contribution to the plasma sheet energy density during the October 2003 superstorm: Geotail/EPIC and IMAGE/LENA observations, *J. Geophys. Res.*, *110*, A09S24, doi:10.1029/2004JA010930.

Peroomian, V., and M. Ashour-Abdalla (1996), Population of the near-Earth magnetotail from the auroral zone, *J. Geophys. Res.*, *101*(A7), 15,387–15,401.

Sánchez, E. R., B. H. Mauk, and C.-I. Meng (1993), Adiabatic vs. non-adiabatic particle distributions during convection surges, *Geophys. Res. Lett.*, *20*(3), 177–180.

Strangeway, R. J., R. E. Ergun, Y. J. Su, C. W. Carlson, and R. C. Elphic (2005), Factors controlling ionospheric outflows as observed at intermediate altitudes, *J. Geophys. Res.*, *110*, A03221, doi:10.1029/2004JA010829.

Tung, Y.-K., C. W. Calson, J. P. McFadden, D. M. Klumpar, G. K. Parks, W. J. Peria, and K. Liou (2001), Auroral polar cap boundary ion conic outflow observed on FAST, *J. Geophys. Res.*, *106*(A3), 3603–3614.

Williams, D. J., R. W. McEntire, C. Schlemm II, A. T. Y. Lui, G. Gloeckler, S. P. Christon, and F. Gliem (1994), Geotail energetic particles and ion composition instrument, *J. Geomagn. Geoelectr.*, *46*, 39–57.

Wilson, G. R., D. M. Ober, G. A. Germany, and E. J. Lund (2001), The relationship between suprathermal heavy ion outflow and auroral electron deposition: Polar Ultraviolet Imager and Fast Auroral Snapshot/Time-of-Flight Energy Angle Mass Spectrometer observations, *J. Geophys. Res.*, *106*(A9), 18,981–18,993.

Wilson, G. R., D. M. Ober, G. A. Germany, and E. J. Lund (2004), Nightside auroral zone and polar cap ion outflow as a function of substorm size and phase, *J. Geophys. Res.*, *109*, A02206, doi:10.1029/2003JA009835.

Winglee, R. M. (1998), Multi-fluid simulations of the magnetosphere: The identification of the geopause and its variation with IMF, *Geophys. Res. Lett.*, *25*(24), 4441–4444.

Yau, A. W., E. G. Shelley, W. K. Peterson, and L. Lenchyshyn (1985), Energetic auroral and polar ion outflow at DE 1 altitudes: Magnitude, composition, magnetic activity dependence, and long-term variations, *J. Geophys. Res.*, *90*(A9), 8417–8432.

Yau, A. W., W. K. Peterson, and E. G. Shelley (1988), Quantitative parameterization of energetic ionospheric ion outflow, in *Modeling Magnetospheric Plasma*, *Geophys. Monogr. Ser.*, vol. 44, edited by T. E. Moore and J. J. H. Waite, pp. 211–217, AGU, Washington, D. C.

Zong, Q.-G., et al. (1998), Energetic oxygen ion bursts in the distant magnetotail as a product of intense substorms: Three case studies, *J. Geophys. Res.*, *103*(A9), 20,339–20,363.

C. W. Carlson and J. P. McFadden, Space Sciences Laboratory, University of California, Berkeley, CA 94720, USA.

S. P. Christon, Focused Analysis and Research, Columbia, MD 21044, USA.

M. R. Collier and T. E. Moore, NASA Goddard Space Flight Center, Code 692, Greenbelt, MD 20771, USA.

M. Nosé, Data Analysis Center for Geomagnetism and Space Magnetism, Graduate School of Science, Kyoto University, Oiwake-cho, Kitashirakawa, Sakyo-ku, Kyoto 606-8502, Japan. (nose@kugi.kyoto-u.ac.jp)

S. Taguchi, Department of Information and Communication Engineering, University of Electro-Communications, 1-5-1 Chofugaoka, Chofu, Tokyo 182-8585, Japan.